Letter

Initial solidification dynamics of spreading droplets

Robin B. J. Koldeweij,[1,2,*] Pallav Kant,[1] Kirsten Harth,[1,3] Rielle de Ruiter,[4] Hanneke Gelderblom,[5] Jacco H. Snoeijer,[1] Detlef Lohse,[1,6] and Michiel A. J. van Limbeek[1,6]

[1]*Physics of Fluids Group, Department of Science and Technology, Max Planck Center Twente for Complex Fluid Dynamics, J. M. Burgers Center for Fluid Dynamics, University of Twente, 7500 AE Enschede, The Netherlands*

[2]*Nano-Instrumentation, TNO, 5612 AP Eindhoven, The Netherlands*

[3]*Institute for Physics, Otto von Guericke University Magdeburg, 39106 Magdeburg, Germany*

[4]*ASML, 5503 LA Veldhoven, The Netherlands*

[5]*Department of Applied Physics, Eindhoven University of Technology, 5600 MB Eindhoven, Netherlands*

[6]*Dynamics of Complex Fluids, Max Planck Institute for Dynamics and Self-Organization, 37077 Göttingen, Germany*

(Received 25 May 2020; accepted 9 November 2021; published 3 December 2021)

When a droplet is brought in contact with an undercooled surface, it wets the substrate and solidifies at the same time. The interplay between the phase transition effects and the contact-line motion, leading to its arrest, remains poorly understood. Here we reveal the early solidification patterns and dynamics of spreading hexadecane droplets. Total internal reflection imaging is employed to temporally and spatially resolve the early solidification behavior. With this, we determine the conditions leading to the contact-line arrest. We quantify the overall nucleation behavior, i.e., the nucleation rate and the crystal growth speed and show its sensitivity to the applied undercooling of the substrate. We also show that for strong enough undercooling it is the rapid growth of the crystals which determines the eventual arrest of the spreading contact line. By combining the Johnson-Mehl-Avrami-Kolmogorov nucleation theory and scaling relations for the spreading, we calculate the temporal evolution of the solid area fraction, which is in good agreement with our observations.

DOI: 10.1103/PhysRevFluids.6.L121601

The spreading of a droplet on an undercooled surface is a very complex phenomenon as it instigates several competing physical processes simultaneously: interfacial deformation, contact-line motion, the associated fluid movement, heat exchange between the droplet and the substrate, and nucleation and growth of a solidified phase within the droplet. Understanding this process is crucial for a broad range of applications that range from ice accretion on roads [1], aircraft [2], and power lines [3] to processes, such as soldering [4,5], thermal spray coating [6], and additive manufacturing [7,8]. So far, several investigations have addressed and characterized the intriguing macroscopic behavior of sessile and impacting droplets on undercooled surfaces. For instance, formation of conical tips during the bulk freezing of a sessile droplet [9] and freezing kinetics along with the final splat morphology of impacting droplets have been investigated in detail [10–16]. Furthermore, nucleation has been studied using top view imaging by applying a thermal gradient to the atmosphere [17,18] or to the substrate [19]. However, nucleation and growth of crystals at the

*Corresponding author. robin.koldeweij@tno.nl

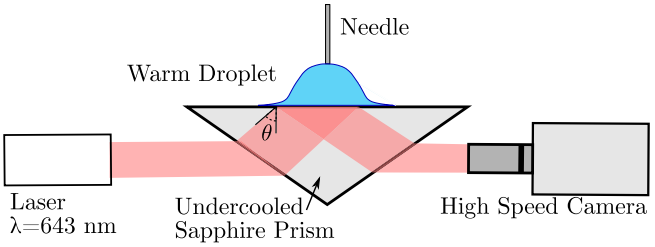

FIG. 1. Schematic of the experimental setup for total internal reflection imaging.

droplet-substrate interface and its subsequent influence on the droplet spreading has received only little attention [20–22].

In this Letter we focus on the interplay between the various phase-transition effects and how they eventually lead to the contact-line arrest. Note that both in this Letter and in Refs. [16,23] the total internal reflection method (TIR) is used. However, in contrast to the study in Ref. [16] where fast waves are studied (<1 ms) inside an *impacting* droplet on a heavily undercooled substrate, here we study the slow arrest of a contact line of a spreading drop on a mildly undercooled substrate. This arrest determines the size and overall shape of the final footprint between the frozen droplet and the substrate. However, due to a lack of direct visualization of the early solidification during droplet spreading, the exact mechanism responsible for contact-line arrest remains debated. So far, various experimental investigations have led to the development of the following explanations: (1) the droplet stops spreading as soon as the contact angle of the spreading liquid reaches the angle of a growing solid front [20], (2) the contact line continues to move until a critical volume solidifies in its vicinity [21], (3) the advancing motion of the droplet lasts until the local temperature falls below a threshold at which the crystal growth speed in the vicinity of the contact line becomes equal to the contact-line velocity [22].

The main object of this Letter is to reveal and explain the sequence of events leading to the contact-line arrest, using TIR imaging. TIR imaging enables us to characterize the influence of substrate undercooling on the crystal nucleation kinetics as well as the tangential crystal growth along the temporally evolving wetted area. Based on these observations we propose a modeling framework that captures the freezing of an evolving droplet footprint by combining classical nucleation theory and droplet spreading dynamics.

A schematic of the experimental setup is depicted in Fig. 1. In a typical experiment, we inflate a droplet of hexadecane to a fixed volume at the tip of a needle. Hexadecane has a melting point of $T_f = 18\,^{\circ}\mathrm{C}$. The droplet, of radius $R_0 = 0.85 \pm 0.05$ mm, is then gently lowered (with negligible approach velocity U) to the horizontal surface of the undercooled sapphire prism with temperature $T_s < T_f$. Upon contact, the droplet spreading and freezing is recorded in the bottom view via TIR using a high-speed camera connected to a long-distance microscope at 30 000 frames per second. Note that, in contrast to the previously described TIR setups that can measure nanometric thin-air films beneath impacting droplets [24–28], our setup allows for direct visualization of the solidified phase. This is achieved by choosing the angle θ of incidence of the laser ($\lambda = 634$ nm) such that total internal reflection occurs not only at the sapphire-air interface, but also at the sapphire-hexadecane interface. The solidified material can be visualized owing to the localized scattering of the evanescent wave by the solid particles. Furthermore, the position of the contact line is clearly visible in the images due to the sudden jump in refractive index between air and hexadecane. A similar setup was recently used in Ref. [16]. Details about the visualization, the experimental setup and the material properties can be found in the Supplemental Material [29] and Ref. [30].

Different types of solidification behavior are observed, for different undercooling $\Delta T = T_f - T_c$. Here, T_c is the droplet-substrate contact temperature, approximated as $T_s + (T_d - T_s)/(1 +$

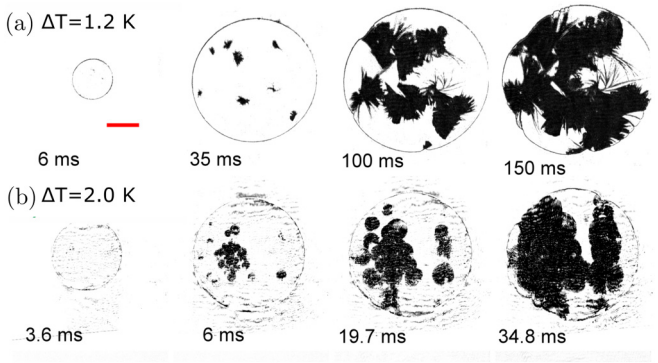

FIG. 2. Characteristic sequences of hexadecane drops spreading on a sapphire prism of varying temperature, the red bar indicates a length of 1 mm: (a) $\Delta T = 1.2$ K: Random nucleation with subsequent dendritic growth. (b) $\Delta T = 2$ K: Continuous nucleation with subsequent radial crystal growth. Note the different timescales in (a) and (b).

e_s/e_d) [31] with $e = \sqrt{k\rho c_p}$ as the thermal effusivity and the subscripts s and d denoting the substrate and the droplet, respectively. Sequences of snapshots in Fig. 2 show the freezing behaviors of droplets spreading on substrates at different ΔTs. For low undercooling [Fig. 2(a)], nucleation initially occurs only at a few locations that are randomly distributed over the droplet footprint. Subsequently, these crystals nuclei grow into needle-shaped structures: columnar dendrites. The nucleation rate and the morphology of the growing crystals change significantly for a slight increase in undercooling. At higher ΔT [Fig. 2(b)], a considerable increase in the amount of crystals is observed. Interestingly, in this case, the enhanced nucleation rate is followed by axisymmetric growth of crystal nuclei, seen as seemingly circular footprints [Fig. 2(b)]. However, a close inspection reveals that these are still constituted of dendritic patterns. Note that the phase-transition effects only initiate after a lag time τ_g [32]. In our experiments, τ_g varies from a few microseconds to a few seconds, respectively, at the largest and smallest of the ΔT employed in our experiments. The increase in the nucleation rate at higher ΔT is directly related to the corresponding decrease in the activation energy for liquid-solid transformation. For the creation of a solid nucleus, this can be considered as the sum of the surface energy between the newly created particle and the bulk, and the released latent energy in the transformed volume of this small nucleus. For a nucleus growing on a surface (heterogeneous nucleation), this critical energy can be approximated as $E_a = (16\pi/3)\gamma_{ls}^3 f(\theta_{ls})/(\Delta g)^2$ [33] with a geometrical correction factor $f(\theta_{ls})$, that depends on the contact angle θ_{ls} of a crystalline deposit with the foreign solid surface [34,35]. Here $\gamma_{ls} = 0.0068$ J m^{-2} [36] is the interfacial tension between the liquid and the solid hexadecane and $\Delta g = \Delta S_{\text{fus}} \Delta T$ is the free-energy difference between the liquid and the solid phases with the entropy of fusion $\Delta S_{\text{fus}} = 6.28 \times 10^5$ J m^{-3} K^{-1} [37]. Note that E_a varies as $(\Delta T)^{-2}$. Accordingly, in our experiments for $\Delta T < 1$ K, we do not observe any nucleation at the experimental timescale (∼5 s). Conversely, the droplet footprint instantly solidifies upon touching the substrate for $\Delta T > 2.9$ K when the E_a decreases with 90%.

To quantify the nucleation kinetics at the early times of droplet spreading, we measure the total number of growing crystals $n_{\text{crystals}}(t)$. Here, we follow the methodology described in Ref. [19]. This involves determining individual crystals at the spatial resolution of our measurements. The result is shown in Fig. 3 where time is rescaled by the capillary time $\tau_c = (\rho R_0^3/\sigma)^{1/2}$ with the surface tension σ between the liquid and the air. For significantly large undercooling ΔT, it follows a power-law behavior, that we will argue to be $n_{\text{crystals}} \propto (t/\tau_c)^{5/2}$.

To rationalize this behavior, we employ classical nucleation theory. The nucleation rate per unit volume is estimated as $J_0 = A \exp(\frac{-E_a[f(\theta_{ls})]}{k_B T_f})$, where k_B is the Boltzmann constant and A is the

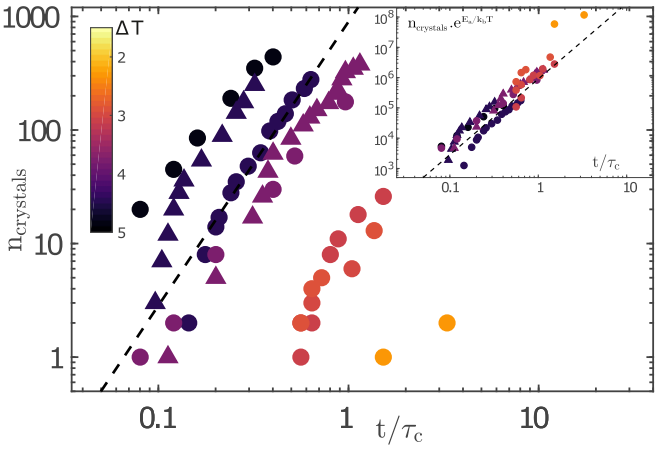

FIG. 3. Number of distinct crystals as function of dimensionless time. Separate experiments are denoted with different symbols. The dashed line (− − −) indicates the scaling [Eq. (1)]. The capillary timescale $\tau_c = (\rho R_0^3/\sigma)^{1/2}$. The color bar shows the temperature difference $\Delta T = T_f - T_c$. The inset shows the same data rescaled with the probability of the formation of a stable crystal nuclei at different ΔTs, $\exp(E_a/k_bT)$.

attempt frequency per unit volume [37–40]. The amount of crystals $n_{\text{crystals}}(t/\tau_c)$ is then obtained by multiplying J_0 by the available volume for nucleation, which is estimated by the wetted area $\pi[R(t)]^2$ times the thermal penetration depth $\delta_{\text{th}} \propto \sqrt{\kappa t}$ with $\kappa = k/(\rho c_p)$ as the thermal diffusivity of the liquid. The number of growing crystals is then described by

$$n_{\text{crystals}} \propto J_0 \int_0^{t/\tau_c} R^2 \delta_{\text{th}} dt. \tag{1}$$

In our experiments, the wetting dynamics of a droplet is indistinguishable from the iso-thermal spreading as found in Refs. [41–46]. The wetting follows the spreading law $R/R_0 \propto (t/\tau_c)^{1/2}$ until the contact line suddenly stops advancing due to the solidification, see the Supplemental Material [29]. To close the problem, we assume that the early-time spreading dynamics of the droplet remains unaffected by the nucleation. Combining this spreading law with Eq. (1), we derive $n_{\text{crystals}} \propto (t/\tau_c)^{5/2}$, which is consistent with the experimental data (Fig. 3). Only for very small ΔT (orange circles in Fig. 3) the amount of crystals does not follow this power law. Due to the low surface energy, τ_g may even be larger than τ_c. Surface impurities can lead to random nucleation in this case. Moreover, a collapse of the experimental data onto a master curve is achieved, Fig. 3 (inset), by rescaling temporal growth of n_{crystals} for different substrate undercooling by the probability of forming stable crystal nuclei at different ΔTs.

We are now in a position to identify the mechanism that leads to the sudden arrest of the moving contact line. Our experiments reveal that the local nature of the interactions between the growing crystals and the moving contact line is one reason that leads to its arrest. Figure 4(a) highlights two distinct events that exemplify the physical mechanism responsible for this contact-line arrest. In the case that a crystal nucleates at the contact line [Fig. 4(a), center panel], it immediately arrests the advancing motion locally. This random event at the moving contact line is caused by local heterogeneities on the substrate. In contrast, a crystal nucleating far away from the contact line [Fig. 4(a), left panel] does not affect its motion immediately, but if its growth catches up with the advancing contact line, it locally arrests the spreading [Fig. 4(a), right panel]. Consequently, in both cases the droplet footprint evolves nonaxisymmetrically.

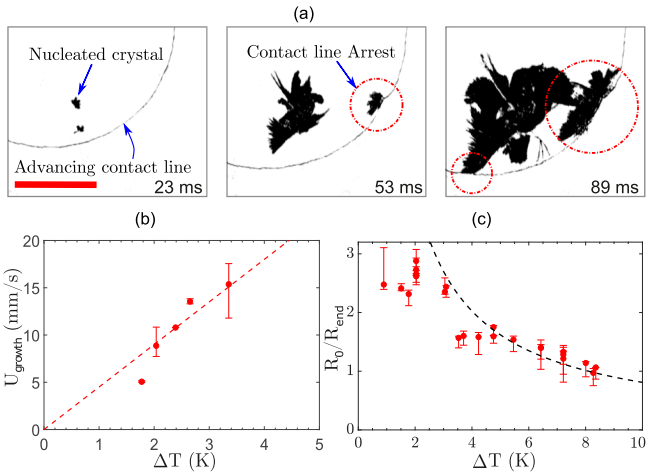

FIG. 4. Contact-line arrest and crystal growth: (a) Nucleation near the contact line, leading to local contact-line arrest (red circles), the red bar indicates a length of 1 mm, $\Delta T = 1.0$ K. (Left panel) Nucleation far away from the contact line. (Center panel) Nucleation close to the contact line leads to contact-line arrest. (Right panel) Crystals growing towards the contact line lead to contact line arrest. (b) Growth velocity as a function of the undercooling ΔT. The error bars indicate the minimal and maximal growth velocity at a certain temperature. The dashed line shows the growth velocity $U_g = \beta\,\Delta T$ with $\beta \approx 4.5\ \mathrm{mm\,s^{-1}\,K^{-1}}$. (c) Radius of arrest versus temperature. − − − is the model of Eq. (2). The error bars show the minimum and maximum radii of a single arrest event.

The contact line was earlier hypothesized to arrest due to the interaction of the crystal growth with the moving contact line [22] with a scaling law for the arrest radius R_{end},

$$R_{\mathrm{end}}/R_0 \propto R_0/(2\tau_c U_g), \tag{2}$$

with U_g as the crystal growth speed, which was approximated as $U_g = \beta\,\Delta T$ [33] where the kinetic undercooling coefficient β (with units $\mathrm{m\,s^{-1}\,K^{-1}}$) is a fitting parameter. Here, we directly obtain the crystal growth speed and with that the undercooling coefficient β by measuring the temporal growth of several crystals after their nucleation at the droplet-substrate contact area for different substrate undercooling. Note that T_c is the natural choice instead of the substrate temperature T_s for this undercooling as the solidification is dictated by the contact temperature. A typical measurement of crystal-growth along the wetted area is included in the Supplemental Material [29]. Notably, the crystal growth speed shows a linear dependence on ΔT [Fig. 4(b)], resulting in $\beta \approx 4.5\ \mathrm{mm\,s^{-1}\,K^{-1}}$. This value is slightly smaller than that for hexadecane spreading on copper obtained from a fit to the data in Ref. [22]. With this independently measured kinetic cooling coefficient, we can now directly test the prediction for contact-line arrest, Eq. (2), by comparing to our measurements. A very good agreement is found, using a prefactor of 0.36 [see Fig. 4(c)]. We point out that the underlying assumption of a linear relationship between crystal growth and undercooling may not be sufficient; this requires further investigation and is beyond the scope of the present Letter. Furthermore, our experimental results significantly deviate from the model at low undercooling $\Delta T < 3$ K. We believe that the implicit assumptions (infinitely small lag time $\tau_g \sim 0$ and high probability of nucleation sites at the contact line) made in the model for droplets spreading on substrates are not applicable at low ΔT. Conversely, for the complete range of ΔT we do not observe any preference of nucleation sites near the contact line. Modeling the contact-line arrest at small undercooling requires to properly account for the statistical nature of the occurrence of nucleation sites on the substrate, which is beyond the scope of this Letter.

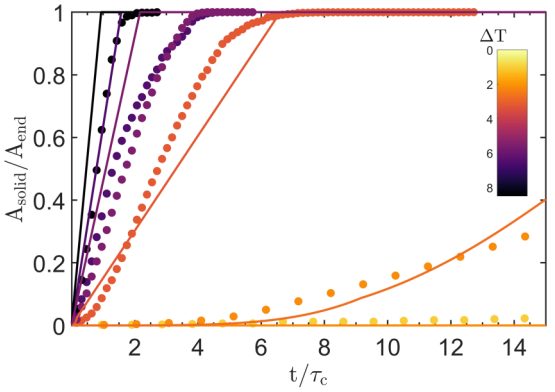

FIG. 5. Time dependence of the fraction of solidified material at the substrate for various temperatures. The solid lines show Eq. (3) for $\Delta T = 2.1$, $\Delta T = 2.7$, $\Delta T = 3.2$, $\Delta T = 5.5$, $\Delta T = 6.5$, $\Delta T = 8.5$ K. A large change in solidification behavior is seen for the model between 2.7 K $< \Delta T <$ 3.2 K.

Finally, we shift our focus to the temporal growth of the solidified area along the droplet-substrate interface. We follow the formulation proposed in Refs. [47,48] for heterogeneous nucleation and growth of the solidified phase on an undercooled surface. It assumes time-independent growth velocity U_g and nucleation rate J_0 with sites equally distributed over the substrate. We use the Johnson-Mehl-Avrami-Kolmogorov (JMAK) equation to determine the two-dimensional growth of the solidified surface fraction as a function of time as $\chi = 1 - \exp(-4\pi N_0 U_g^2 t^2)$. The amount of crystals per area is estimated as $N_0 = \int_0^t J_0 \delta_{\text{th}} dt$. As the droplet continues to spread over the substrate, the area available for nucleation increases. Hence, we rescale the JMAK equation by the instantaneous wetted area $R(t)^2/R_{\text{end}}^2$ to find

$$\frac{A_{\text{solid}}}{A_{\text{end}}} = \left[1 - \exp\left(-\frac{8\pi}{3} J_0 \delta_{\text{th}} U_g^2 t^3\right)\right]\left(\frac{R(t)}{R_{\text{end}}}\right)^2, \tag{3}$$

where we use the arrest criterion [Eq. (2)] to obtain R_{end}.

The evolution of the solidified area fraction for various surface undercoolings is shown in Fig. 5. Below $\Delta T < 2.5$ K, the slow nucleation leads to a very slow increase in solidified area fraction. At higher ΔT, both the nucleation rate and the crystal growth speed increase. Consequently, the solidified area fraction grows faster. For even higher undercooling $\Delta T > 4.4$ K, the solidified fraction growth rate matches the spreading of the droplet, thus, $A_{\text{solid}}/A_{\text{end}} \approx [R(t)/R_{\text{end}}]^2$. Even though the JMAK equation has its limitations for when the amount of growing nuclei is limited [49] and although our approach does not take potential defects outside of neighboring transformed areas in to account, we find that Eq. (3) agrees reasonably with the experimental data over a wide range of ΔT. The only adjustable parameter is the geometrical factor $f(\theta_{ls})$ since the average nucleus contact angle is not directly measurable [50]. From a fit to the data, we find $f(\theta_{ls}) \approx 0.12$, which implies an average nucleus contact angle of $\theta_{ls} \approx 55^\circ$. It must be pointed out that for undercooling below 2.5 K, the model does not predict any solidification within the typical timescale of experiments. This observation corroborates our conjecture that it is impurities that cause nucleation and growth in this temperature range.

To summarize, we directly visualized the surface solidification during spreading of hexadecane droplets on an undercooled sapphire surface using high-speed TIR imaging. Two distinct solidification behaviors are observed, which are explained by classical nucleation theory. The number of crystals in a spreading droplet scale with $n_{\text{crystals}} \propto (t/\tau_c)^{5/2}$. Furthermore, we reveal that the arrest velocity is approximately equal to the crystal growth velocity determined by the undercooling. This direct observation is in line with the model developed in Ref. [22]. However, it is not valid for

very weak undercooling since the nucleation happens randomly over the surface. Apart from the processes near the contact line, we reveal that the crystal growth speed directly depends on the contact temperature T_c, rather than on the initial temperature of the substrate T_s. Finally, we showed that the two-dimensionalJMAK equation, rescaled for the time-dependent contact area reasonably predicts the temporal growth of the solidified area fraction of a spreading droplet. Our results give insight into both local and overall solidification processes near the contact line of a hexadecane droplet and are equally applicable to other liquids, such as water and liquid-metals, for example [19]. The visualization method opens an experimental pathway of elucidating solidification behavior near substrates on time-resolved macro- and microscopic scales. This technique can be used to directly measure the early solidification behavior for many relevant applications in manufacturing.

We acknowledge funding by the Max Planck Center Twente, R.B.J.K. acknowledges funding by the TNO ERP programme 3D nanomanufacturing. K.H. acknowledges funding by German Science Foundation DFG within Grant No. HA8467/1-1. D.L. acknowledges the ERC Advanced Grant No. DDD 740479. We thank M. van der Ouderaa and S. Kölling for participating in the experiments.

[1] H. Chen, Y. Wu, H. Xia, B. Jing, and Q. Zhang, Review of ice-pavement adhesion study and development of hydrophobic surface in pavement deicing, J. Traffic Transp. Eng. (English ed. **5**, 224 (2018).
[2] T. Cebeci and F. Kafyeke, Aircraft Icing, Annu. Rev. Fluid Mech. **35**, 11 (2002).
[3] M. Farzaneh, *De-icing Tech. Overhead Lines* (Chicoutimi, 2008), Vol. 84, Chap. 6, p. 381.
[4] D. J. Hayes, D. B. Wallace, and W. Royall Cox, MicroJet printing of solder and polymers for multi-chip modules and chip-scale packages, in *Proceedings-SPIE the International Society for Optical Engineering* (Citeseer, 1999), pp. 242–247.
[5] D. Attinger, Z. Zhao, and D. Poulikakos, An experimental study of molten microdroplet surface deposition and solidification: Transient behavior and wetting angle dynamics, J. Heat Transfer **122**, 544 (2002).
[6] S. Chandra and P. Fauchais, Formation of solid splats during thermal spray deposition, J. Therm. Spray Technol. **18**, 148 (2009).
[7] M. Vaezi, H. Seitz, and S. Yang, A review on 3D micro-additive manufacturing technologies, Int. J. Adv. Manuf. Technol. **67**, 1721 (2013).
[8] C. Visser, R. Pohl, C. Sun, G. Römer, B. Huis In 'T Veld, and D. Lohse, Toward 3D printing of pure metals by laser-induced forward transfer, Adv. Mater. **27**, 4087 (2015).
[9] O. R. Enríquez, Á. G. Marín, K. G. Winkels, and J. H. Snoeijer, Freezing singularities in water drops, Phys. Fluids **24**, 091102 (2012).
[10] M. Pasandideh-Fard, V. Pershin, S. Chandra, and J. Mostaghimi, Splat shapes in a thermal spray coating process: Simulations and experiments, J. Therm. Spray Technol. **11**, 206 (2002).
[11] A. I. Fedorchenko and A. B. Wang, Non-equilibrium solidification of the molten metal droplets impacting on a solid surface, Int. J. Heat Mass Transf. **50**, 2463 (2007).
[12] W. Kong and H. Liu, A theory on the icing evolution of supercooled water near solid substrate, Int. J. Heat Mass Transf. **91**, 1217 (2015).
[13] E. Ghabache, C. Josserand, and T. Séon, Frozen Impacted Drop: From Fragmentation to Hierarchical Crack Patterns, Phys. Rev. Lett. **117**, 074501 (2016).
[14] V. Thiévenaz, T. Séon, and C. Josserand, Solidification dynamics of an impacted drop, J. Fluid Mech. **874**, 756 (2019).
[15] M. V. Gielen, R. de Ruiter, R. B. Koldeweij, D. Lohse, J. H. Snoeijer, and H. Gelderblom, Solidification of liquid metal drops during impact, J. Fluid Mech. **883**, A32 (2020).
[16] P. Kant, R. B. Koldeweij, K. Harth, M. A. van Limbeek, and D. Lohse, Fast-freezing kinetics inside a droplet impacting on a cold surface, Proc. Natl. Acad. Sci. USA **117**, 2788 (2020).
[17] C. Gurganus, A. B. Kostinski, and R. A. Shaw, Fast imaging of freezing drops: No preference for nucleation at the contact line, J. Phys. Chem. Lett. **2**, 1449 (2011).

[18] C. Tropea, M. Schremb, and I. V. Roisman, Physics of SLD Impact and Solidification, in *7th European Conference for Aeronautics and Space Sciences, Milan, Italy, 2017* (EUCASS, Rhode-St-Genese, Belgium, 2017), p. EUCASS2017–512 7TH.
[19] C. Gurganus, A. B. Kostinski, and R. A. Shaw, High-speed imaging of freezing drops: Still no preference for the contact line, J. Phys. Chem. C **117**, 6195 (2013).
[20] S. Schiaffino and A. A. Sonin, On the theory for the arrest of an advancing molten contact line on a cold solid of the same material, Phys. Fluids **9**, 2227 (1997).
[21] H. Jones, Cooling, freezing and substrate impact of droplets formed by rotary atomization, J. Phys. D. Appl. Phys. **4**, 1657 (1971).
[22] R. de Ruiter, P. Colinet, P. Brunet, J. H. Snoeijer, and H. Gelderblom, Contact line arrest in solidifying spreading drops, Phys. Rev. Fluids **2**, 043602 (2017).
[23] P. Kant, H. Müller-Groeling, and D. Lohse, Pattern Formation During the Impact of a Partially Frozen Binary Droplet on a Cold Surface, Phys. Rev. Lett. **125**, 184501 (2020).
[24] J. Kim, Spray cooling heat transfer: The state of the art, Int. J. Heat Fluid Flow **28**, 753 (2007).
[25] J. M. Kolinski, S. M. Rubinstein, S. Mandre, M. P. Brenner, D. A. Weitz, and L. Mahadevan, Skating on a Film of Air: Drops Impacting on a Surface, Phys. Rev. Lett. **108**, 074503 (2012).
[26] M. Khavari, C. Sun, D. Lohse, and T. Tran, Fingering patterns during droplet impact on heated surfaces, Soft Matter **11**, 3298 (2015).
[27] M. A. Van Limbeek, M. Shirota, P. Sleutel, C. Sun, A. Prosperetti, and D. Lohse, Vapour cooling of poorly conducting hot substrates increases the dynamic Leidenfrost temperature, Int. J. Heat Mass Transf. **97**, 101 (2016).
[28] M. Shirota, M. A. van Limbeek, D. Lohse, and C. Sun, Measuring thin films using quantitative frustrated total internal reflection (FTIR), Eur. Phys. J. E **40**, 54 (2017).
[29] See Supplemental Material at http://link.aps.org/supplemental/10.1103/PhysRevFluids.6.L121601 for details about the visualization, the experimental setup, and the material properties (2021).
[30] G. Osnabrugge, S. Leedumrongwatthanakun, and I. M. Vellekoop, A convergent Born series for solving the inhomogeneous Helmholtz equation in arbitrarily large media, J. Comput. Phys. **322**, 113 (2016).
[31] H. S. Carslaw and J. C. Jaeger, *Conduction of Heat in Solids*, Vol. 2 (Oxford Science, Oxford, 2016), pp. 87–89.
[32] O. Söhnel and J. W. Mullin, Interpretation of crystallization induction periods, J. Colloid **123**, 43 (1988).
[33] S. H. Davis, *Theory of Solidification* (Cambridge University Press, Cambridge, UK, 2001).
[34] J. W. Mullin, *Crystallisation*, 4th ed. (Butterworth-Heinemann, Oxford, 2007), Vol. 6, pp. 201–202.
[35] M. Dorrestijn, S. Jung, C. M. Megaridis, D. Raps, A. Das, and D. Poulikakos, Are Superhydrophobic Surfaces Best for Icephobicity? Langmuir **27**, 3059 (2011).
[36] M. J. Oliver and P. D. Calvert, Homogeneous nucleation of n-alkanes measured by differential scanning calorimetry, J. Cryst. Growth **30**, 343 (1975).
[37] A. B. Herhold, D. Ertaş, A. J. Levine, and H. E. King, Jr., Impurity mediated nucleation in hexadecane-in-water emulsions, Phys. Rev. E **59**, 6946 (1999).
[38] K. F. Kelton, A. L. Greer, and C. V. Thompson, Transient nucleation in condensed systems, J. Chem. Phys. **79**, 6261 (1983).
[39] D. T. Wu, Nucleation Theory, Solid State Phys. **50**, 37 (1996).
[40] A. B. Herhold, H. E. King, and E. B. Sirota, A vanishing nucleation barrier for the n-alkane rotator-to-crystal transformation, J. Chem. Phys. **116**, 9036 (2002).
[41] L. H. Tanner, The spreading of silicone oil drops on horizontal surfaces, J. Phys. D: Appl. Phys. **12**, 1473 (1979).
[42] A. L. Biance, C. Clanet, and D. Quéré, First steps in the spreading of a liquid droplet, Phys. Rev. E **69**, 016301 (2004).
[43] J. C. Bird, S. Mandre, and H. A. Stone, Short-Time Dynamics of Partial Wetting, Phys. Rev. Lett. **100**, 234501 (2008).
[44] K. G. Winkels, J. H. Weijs, A. Eddi, and J. H. Snoeijer, Initial spreading of low-viscosity drops on partially wetting surfaces, Phys. Rev. E **85**, 055301(R) (2012).

[45] B. B. Stapelbroek, H. P. Jansen, E. S. Kooij, J. H. Snoeijer, and A. Eddi, Universal spreading of water drops on complex surfaces, Soft Matter **10**, 2641 (2014).
[46] S. Wildeman, C. W. Visser, C. Sun, and D. Lohse, On the spreading of impacting drops, J. Fluid Mech. **805**, 636 (2016).
[47] E. Dutra Zanotto, Surface nucleation in a diopside glass, J. Non. Cryst. Solids **130**, 217 (1991).
[48] M. Fanfoni and M. Tomellini, The Johnson-Mehl-Avrami-Kolmogorov model: A brief review, Il Nuovo Cimento D. **20**, 1171 (1998).
[49] M. Todinov, On some limitations of the johnson–mehl–avrami–kolmogorov equation, Acta Mater. **48**, 4217 (2000).
[50] A. Määttänen and M. Douspis, Estimating the variability of contact parameter temperature dependence with the Monte Carlo Markov Chain method, GeoResJ **4**, 46 (2014).